RSC Advances

PAPER

View Article Online
View Journal | View Issue

Cite this: *RSC Adv.*, 2019, **9**, 26843

The fabrication of an Ni_6MnO_8 nanoflake-modified acupuncture needle electrode for highly sensitive ascorbic acid detection

Hongliang Jia, Jianwei Zhao, * Lirong Qin, Min Zhao and Gang Liu

Received 22nd May 2019
Accepted 9th August 2019

DOI: 10.1039/c9ra03850g

rsc.li/rsc-advances

The current work describes the use of a steel acupuncture needle as an electrode substrate in order to construct an Ni_6MnO_8 nanoflake layer-modified microneedle sensor for highly sensitive ascorbic acid detection. For the purpose of constructing the functionalized acupuncture needle, first, a carbon film was layered on the needle surface as the seed layer. Subsequently, a straightforward hydrothermal reaction-calcination process was employed for the growth of Ni_6MnO_8 nanoflakes on the needle to function as a sensing interface. Electrochemical investigations illustrated the fact that the Ni_6MnO_8 nanoflake-altered acupuncture needle electrode manifested outstanding efficiency toward the amperometric identification of ascorbic acid. In addition, the electrode manifested elevated sensitivity of 3106 μA mM^{-1} cm^{-2}, detection limit of 0.1 μM, and a broad linear range between 1.0 μM and 2.0 mM. As demonstrated by the results, the Ni_6MnO_8 nanoflake-modified acupuncture needle constitutes a potentially fresh platform to construct non-enzymatic ascorbic acid sensors.

Introduction

Ascorbic acid (AA), which is termed as vitamin C, refers to a kind of anti-oxidant that is present in a number of biological species that take part in different kinds of crucial biological reactions.[1] Moreover, AA helps promote the healthy growth of cells, aids in calcium absorption as well as normal tissue development, and functions as a medication for scurvy, drug poisoning, liver illness, allergic reactions and atherosclerosis.[2] In this context, the development of a straightforward and rapid methodology to determine AA with elevated selectivity and sensitivity is preferred for both diagnostic and food safety applications.[3] Different kinds of analytical methodologies including chemiluminescence,[4] fluorescence,[5] electrophoresis,[7] liquid chromatography,[6] and electrochemical methodologies[8] have been employed for the purpose of investigating the ascorbic acid content in drugs, foods and plants. Among these approaches, the electrochemical methodologies have presented feasible, straightforward and affordable identification with elevated sensitivity.[9] Nevertheless, enzymatic sensors suffer from a number of potential flaws, such as stereotyped shapes, instability and poor reproducibility on account of the intrinsic characteristics of enzymes. As a result, the development of non-enzymatic AA sensors that have excellent characteristics coupled with a well-designed shape is desired.[10]

Two-dimensional (2D) nanoflakes are significantly interesting due to their exclusive characteristics, which include not only a large specific surface area, but also rich structural diversity and exclusive electronic characteristics.[11] NiO nanoflakes are among the most appealing inorganic substances with applications in catalysis, ion exchange, molecular adsorption, biosensing, and power conservation.[12] Recently, the electrochemical uses of NiO in detecting glucose,[13] ascorbic acid,[14] and H_2O_2 (ref. 15) and in gas sensing[16] have been indicated to have applications in a variety of areas. Likewise, MnO_2 nanosheets are also counted among the key types of redox-active 2D nanomaterials. They have extensive applications in biosensing due to their reasonable water solubility, catalytic activity and outstanding biocompatibility.[17] Taking into consideration the fact that Ni-based as well as Mn-based oxides manifest high electrochemical efficiencies, the corresponding mixed metal oxides would be expected to have better characteristics. In particular, Ni_6MnO_8 shows more advantages and better application prospects due to its easily available raw materials, simple preparation methods, high electroactivity and excellent stability.

Acupuncture is considered a pivotal component of Eastern medicine; it has the functions of relieving pain, warming the meridians and promoting the blood flow through the application of an acupuncture needle into the physical body of the patient. In addition, the stainless-steel-based needle is not only affordable but also convenient to use and is put to common uses in actual applications.[18] Due to its high conductivity, small size, and needle-like edge, the electrode, based on the acupuncture needle, can be put to use for micro-volume

School of Physical Science and Technology, Southwest University, Chongqing 400715, P. R. China. E-mail: zhaojw@swu.edu.cn; Fax: +86 23 68254608; Tel: +86 23 68252355

specimens or *in vivo* analysis. Zhou *et al.* developed a nonenzymatic H_2O_2 microsensor on the basis of an acupuncture needle functionalized with MoS_2/Pt nanocomposites.[19] Niu *et al.* selected an acupuncture needle as the basic electrode to further modify using gold nanoparticles and graphene for the sensitive determination of rutin.[20] Therefore, needle electrodes have promising applications in constructing electrochemical sensing platforms. In the current research work, we put forward a novel AA sensor on the basis of a steel acupuncture needle as the electrode substrate to construct an Ni_6MnO_8 nanoflake layer. The presented sensor manifested a number of outstanding characteristics ascribed to the synthetic impact of the mixed metal oxides and the thin nanoflake structures; furthermore, the remarkable acupuncture needle improved the electrochemical response to AA to a significant extent.

Experimental

Reagents and instrumentation

Ascorbic acid, uric acid, glucose, L-tyrosine, and dopamine were obtained from Sigma-Aldrich. Nickel nitratehexahydrate together with manganese chloride tetrahydrate and other chemicals of analytical grade was purchased from Chongqing Chuandong Chemical Company. Deionized water was used throughout the entire assay. A CHI 660E electrochemical workstation (CH Instruments, China) was used for electrochemical identification using a 3-electrode system, which comprised an altered working electrode, a Pt counter electrode, and an Ag/AgCl reference electrode. Each and every experiment was performed at an ambient temperature (23 ± 1 °C). The characterization of the morphologies of our synthesized products was carried out with the help of scanning electrode microscopy (SEM, JEOL JSM 7100F) as well as the transmission electron microscopy (TEM, JEM 2010); the analysis of the elemental composition was carried out with the help of X-ray diffraction (XRD, TD-3500) as well as energy dispersive X-ray spectroscopy (EDS, Aztec X-Act).

Fabrication of Ni_6MnO_8 nanoflake-modified needle electrode

Prior to synthesis, the cleaning of the stainless steel needle put to use for acupuncture (diameter: 0.25 mm, length: 13 mm) was done with the help of sonication in ethanol and deionized water for a period of fifteen minutes each. Subsequently, the Ni_6MnO_8 nanoflake-modified needle electrode was prepared, as demonstrated in Fig. 1. Specifically, the cleaned steel needle was soaked in 0.03 M (mol L^{-1}) glucose solution for fifteen hours, followed by annealing in argon for a period of three hours at a temperature of 500 °C. Without this step, that is, without the carbon film as the seed layer, the Ni_6MnO_8 nanoflakes grown on the surface of the steel needle would not be well-distributed. As for the synthesis of the Ni_6MnO_8 nanoflakes, 0.58 g of $Ni(NO_3)_2 \cdot 6H_2O$ together with 0.97 g of $MnCl_2 \cdot 4H_2O$, 0.21 g of methenamine and 0.09 g of urea was dissolved in 30 mL of deionized water with continuous stirring. In addition, the solution was transferred into a Teflon-lined stainless autoclave, and the pre-treated stainless steel needle was placed in it as well. Subsequently, the autoclave was sealed and maintained at a temperature of 120 °C for a period of six hours. Subsequent to cooling it down to the room temperature, the acupuncture needle was washed with ethanol and deionized water a number of times, followed by annealing in air for a period of two hours at a temperature of 450 °C. In the meantime, the powder deposited in the solution during the hydrothermal procedure was also collected, followed by washing and annealing under the same conditions for XRD characterization. Eventually, the modified steel needle was encapsulated by coating with epoxy resin directly in the middle areas, leaving the tip with about 10 mm of length for the electrochemical measurement.

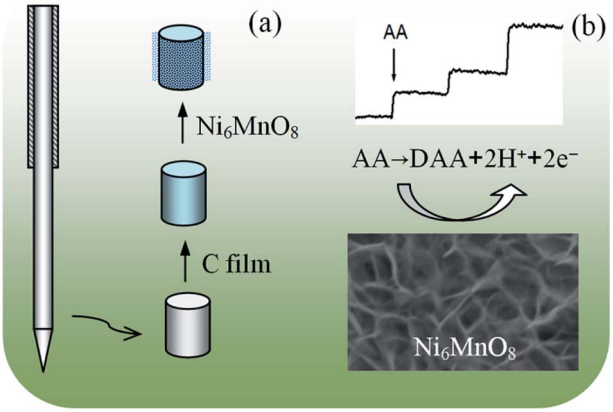

Fig. 1 (a) Fabrication process for the preparation of Ni_6MnO_8/C/needle. (b) Schematic illustration of the Ni_6MnO_8 nanoflakes for the detection of AA.

Results and discussion

Characterization of the nanoflake-modified electrode

Fig. 2a shows an overview SEM image of the product grown on the tip of the acupuncture needle. Evidently, the integrated and concentrated nanoflakes were distributed on the surface of the needle. The high-magnification SEM images suggest that the product possessed flake-like morphology[21–23] (Fig. 2b and c), with a lateral size ranging between 50 and 200 nm, and was a few nanometers thick. During the hydrothermal reaction, methenamine and urea were the alkali sources and generated OH^- to react with the metal ions. Then, they served as the structural guide and directed the self-assembly of the flake-like structures. These tiny flakes were interlaced, which created an extremely porous 3D network on the substrate, accordingly offering an extensive specific surface area.[24] Fig. 3 demonstrates a typical TEM image of the nanoflakes, and the flake-like nanostructures can be observed quite clearly. Furthermore, the respective SAED pattern (inset of Fig. 3) reveals that the nanoflakes are polycrystalline. The diffraction rings in the SAED pattern correspond to the (222) and (400) crystal planes of the cubic structural Ni_6MnO_8.

For the purpose of analysing the elemental composition of the prepared nanoflakes, the EDS spectrum of the sample was obtained, which is presented in Fig. 4a. It suggested that the

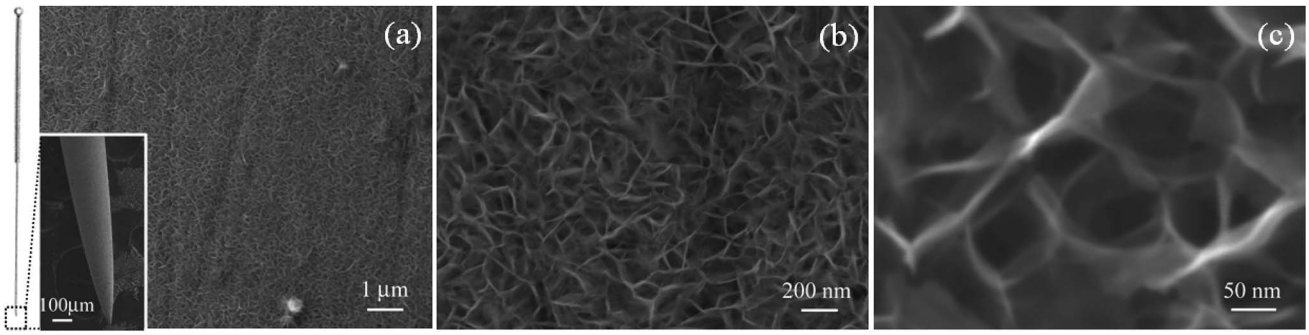

Fig. 2 (a) Low-magnification SEM image of Ni_6MnO_8 nanoflakes; inset: SEM image of the modified acupuncture needle. (b and c) High-magnification SEM images of the Ni_6MnO_8 nanoflakes.

nanoflakes comprise Ni, Mn and O. The weak C signal originated from the carbon film coated on the needle. Using additional quantitative analysis, the average atomic ratio of Ni : Mn that the EDS system provided was determined to be approximately 6 : 1, and it was consistent with the value of Ni_6MnO_8. Owing to the amount of nanoflakes grown on the acupuncture needle being insufficient for XRD characterization, the powder deposited in the solution during the hydrothermal process was also collected, followed by annealing under the same conditions. SEM and EDS analyses suggested that the powder possessed similar morphology and elemental composition to those of the nanoflakes grown on the acupuncture needle. The XRD pattern of the powder was also obtained, and the findings are illustrated in Fig. 4b. The three typical characteristic peaks at approximately $2\theta = 37.4^\circ$, 43.5°, and 63.1° were attributed to the (222), (400), and (440) diffraction modes of the face-centered cubic structure of Ni_6MnO_8, respectively.[25,26] This result indirectly verified that the nanoflakes grown on the needle must be Ni_6MnO_8. EDS in the area mapping mode was conducted to detect the spatial distribution of specific elements. Fig. 5 indicates that O, Ni and Mn are distributed within the nanoflakes, confirming again the formation of Ni_6MnO_8.

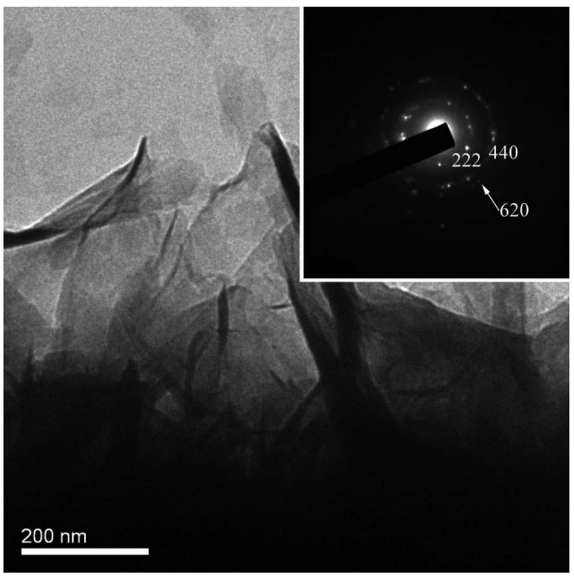

Fig. 3 TEM image of the Ni_6MnO_8 nanoflakes; inset: the corresponding SAED pattern.

Properties of the nanoflake-modified electrode

The steel acupuncture needle modified with the Ni_6MnO_8 nanoflake layer can be directly applied as a sensor electrode for detecting AA. In addition, the electrochemical efficiency of this

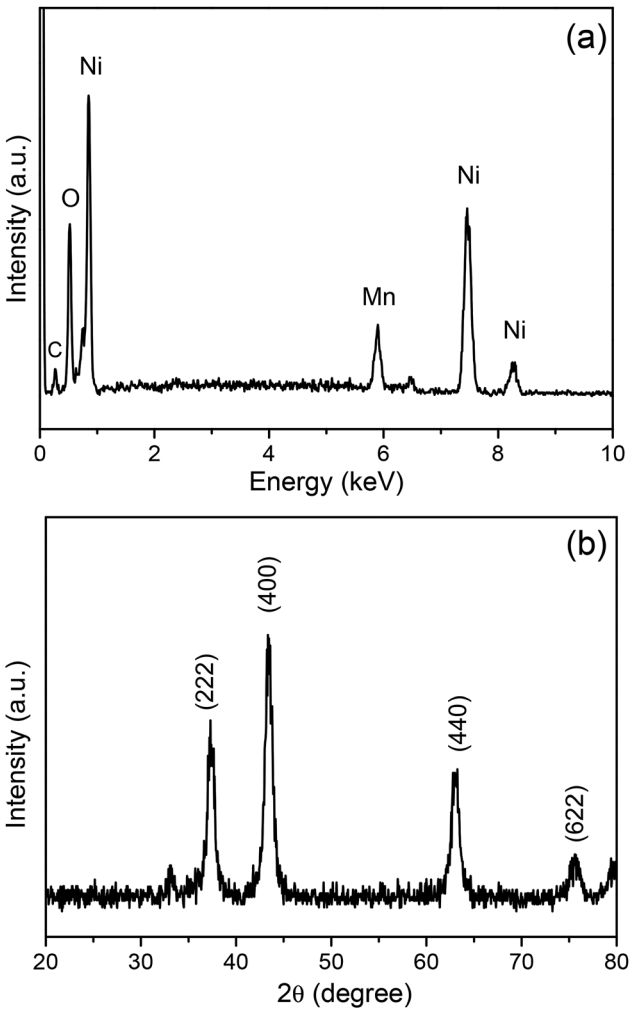

Fig. 4 (a) EDS spectrum and (b) XRD pattern of the Ni_6MnO_8 nanoflakes.

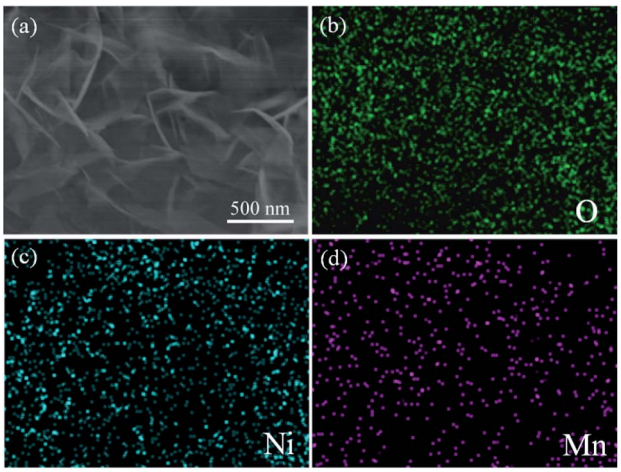

Fig. 5 (a) An SEM image of the Ni_6MnO_8 nanoflakes; (b–d) the elemental chemical maps of O, Ni, and Mn, respectively.

needle electrode was examined with cyclic voltammetry (CV) in a 0.1 M NaOH solution over a potential range between 0.1 and 0.6 V at the scan rate of 100 mV s^{-1}. As evident from Fig. 6a, in comparison with the result for the system with no AA, the oxidation peak increases as 1.0 mM AA is introduced into the solution. This result suggests that the Ni_6MnO_8 nanoflakes have robust electrocatalytic activity with regard to the oxidation of AA. Furthermore, it is possible to assign the effectively defined redox peak in the research potential range to the electrochemical redox reactions of Ni(II)/Ni and Mn(IV)/Mn(II) on the electrode surface.[12,27] Herein, AA oxidation involves the removal of two hydrions and two electrons to form dehydroascorbic acid ($C_6H_6O_6$), which shows resistance to a reversible change in an alkaline solution.[28] The latent catalytic activity of Ni_6MnO_8 for AA oxidation can be explained in accordance with the scheme presented below:

$$Ni(II) + Mn(IV) + 2C_6H_8O_6 \rightarrow Ni + Mn(II) + 4H^+ + 2C_6H_6O_6 \quad (1)$$

$$H^+ + OH^- \rightarrow H_2O \quad (2)$$

$$Ni \rightarrow Ni(II) + 2e,\ Mn(II) \rightarrow Mn(IV) + 2e \quad (3)$$

The kinetic and transport attributes of the response were additionally studied through cyclic voltammetry with varying scan rates. Fig. 6b shows the CVs of the modified electrode in a 0.1 M NaOH solution containing 0.5 mM AA at varying scan rates. It is quite fascinating to observe that the oxidation peak currents are in proportion to the square root of the scan rate between 50 and 280 mV s^{-1}, which indicates that the diffusion-controlled process occurs at the altered electrode.[29] This result suggests reliable and fast electron transfer kinetics at the surface of the electrode, which is advantageous for amperometric sensing.

An amperometric technique was used for the purpose of evaluating the electrode for AA detection. Fig. 7a and b both show the common current–time feedbacks of the needle

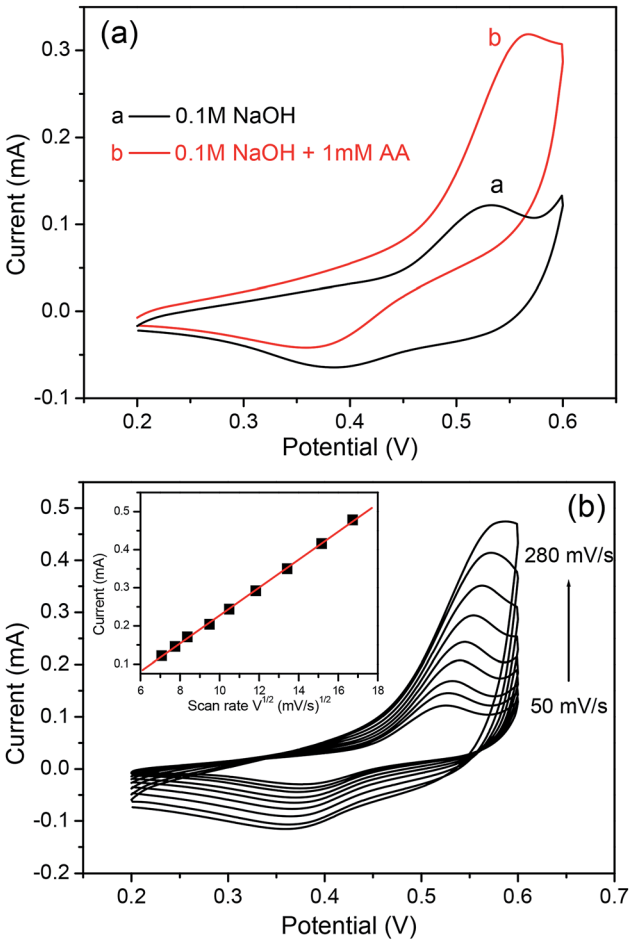

Fig. 6 (a) CV curves of the Ni_6MnO_8 nanoflake-modified electrode in the absence (curve a) and presence (curve b) of AA in 0.1 M NaOH solution. (b) Typical CVs of the modified electrode in 0.1 M NaOH solution containing 0.5 mM AA at different scan rates (from 50 to 280 mV s^{-1}). Inset: plots of peak currents *vs.* $\nu^{1/2}$.

electrode subsequent to successively adding AA into a 0.1 M NaOH solution at a constant potential of 0.55 V. Throughout the test, the solution was stirred at a constant pace with the help of a magnetic stirrer to accelerate mixing. Upon injecting AA, a fast-paced current feedback was observed and a stable value was attained in under 5 s, which illustrated a sensitive feedback to the modification in the AA concentration. Besides, the inset in Fig. 7b indicates the linear association existing between the concentration of AA and the current. In addition, an extensive linear response range of the electrode to the AA concentration was present between 1.0 μM and 2.0 mM. Besides this, the linear regression equation is I (μA) = 21.598 + 146.32 C (mM) with a correlation coefficient of 0.9962. The constraint of identification was approximated as 0.1 μM at a signal/noise ratio of 3. Further determination of the sensitivity could be increased to 3106 μA mM^{-1} cm^{-2}. Table 1 demonstrates a comparison of the efficiency of the Ni_6MnO_8 nanoflake-altered needle electrode shown herein with those of the other AA sensors prepared using nanomaterials. It was evident that the available electrode material presented outstanding

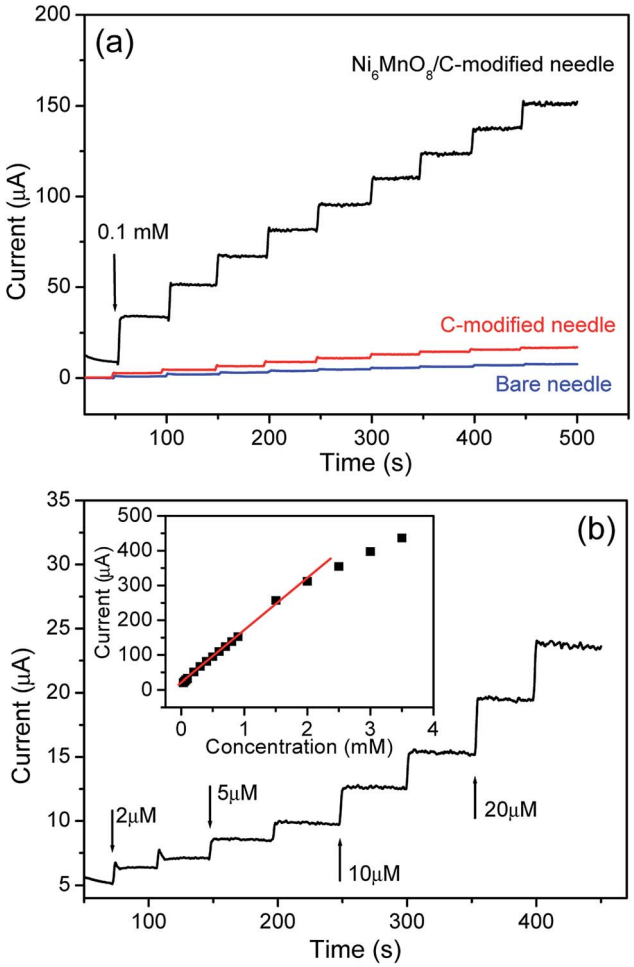

Fig. 7 (a) Typical current–time responses for the Ni_6MnO_8 nanoflake-modified electrode, the C-modified electrode, and the bare needle electrode to successive additions of 0.1 mM AA in a stirring 0.1 M NaOH solution at an applied potential of 0.55 V *vs.* Ag/AgCl. (b) The current–time responses for the Ni_6MnO_8 nanoflake-modified electrode to successive additions of different concentrations of AA; inset: the linear relationship between the catalytic current and the concentration of the Ni_6MnO_8 nanoflakes.

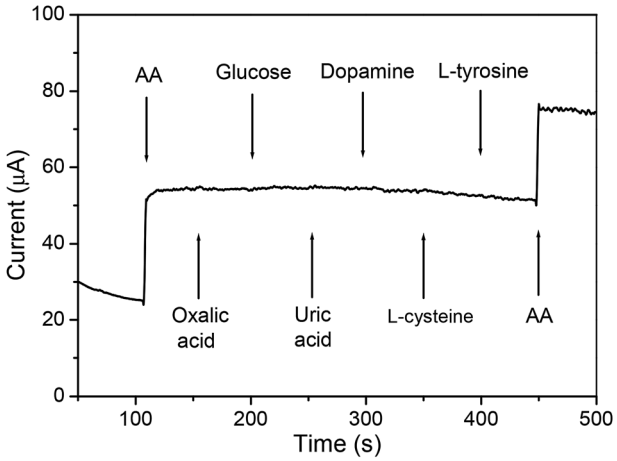

Fig. 8 Amperometric curve for the addition of 0.1 mM AA, oxalic acid, glucose, uric acid, dopamine, L-cysteine, L-tyrosine and 0.1 mM AA in 10 mL 0.1 M NaOH solution.

electrochemical efficiency regarding its elevated sensitivity, low detection limit, and extensive linear range. These ideal attributes of the developed electrode are due to the particular structure of the Ni_6MnO_8 nanoflakes modified on the acupuncture needle. At first, the highly dense nanoflakes could provide an extensive surface region for solution percolation, causing a rise in the electrochemically active surface sites, accordingly giving rise to outstanding sensing efficiency.[10,29] Second, a synergetic effect from the combination of NiO and MnO_2 likely augmented the catalytic efficiency of the nanoflakes, further promoting the oxidation of AA.[35] In contrast, it is evident from Fig. 6a that the needle electrode without the Ni_6MnO_8 nanoflakes in our experiment exhibits quite a low function for AA oxidation. Eventually, the direct development of nanoflakes onto the needle electrode enabled reasonable mechanical binding[22] as well as the electric connection of the active substance to the current collector.

The examination of the impact of common interfering species on the Ni_6MnO_8 nanoflake layer-modified microneedle sensor was also carried out. In accordance with Fig. 8, after the addition of 0.1 mM AA into a 10 mL 0.1 M NaOH solution, there was significant increase in the current with immense response sensitivity. As compared with AA, upon the addition of 0.1 mM oxalic acid, glucose, uric acid (UA), dopamine, L-cysteine and L-tyrosine, we did not notice any apparent signal from these materials. In this manner, a conclusion can be reached that this Ni_6MnO_8 nanoflake-modified needle electrode put forward in

Table 1 Comparison of different amperometric sensors for the determination of ascorbic acid

Type of electrode	Sensitivity ($\mu A\ mM^{-1}\ cm^{-2}$)	Linear range (μM)	Detection limit (μM)	Reference
GO-XDA-Mn_2O_3 nanocomposite	655.74	10–8000	0.6	28
CuS@PB composites	256.91	5–3875	0.24	30
NiO nanosheets@Tr-rGO	177.83	0.25–13 100	0.25	31
$NiCoO_2$/C	549.3	20–2410	0.5	32
3DGF/CuO nanoflowers	2060	0.43–200	0.43	33
Ascorbate oxidase/PEDOT-SL film	80.4	2–14 000	0.464	34
Nanoporous Fe_2O_3/Au film	1281.9	25–10 000	1.0	10
Ni_6MnO_8 nanoflakes/C/steel needle	3106	1–2000	0.1	This work

Table 2 Determination of AA in vitamin C tablets ($n = 3$)

Sample	Detected/μM	Added/μM	Found/μM	Recovery, %
1	201.1	200	391.5	97.6
2	382.6	200	578.6	99.3
3	516.5	200	692.1	96.5

the current research work shows reasonable selectivity to AA. As revealed by former reports, Ni-based sensors are capable of detecting glucose, UA, and dopamine on the basis of the involvement of Ni(II) as well as Ni(III) species as an electron transfer mediator.[36–39] Herein, we think the incorporated Mn element could inhibit the reaction of Ni(II)/Ni(III), decreasing the oxidative ability of Ni(II). In contrast, AA, a mild reducing agent, can be easily oxidized than other interfering species with the loss of two electrons to form dehydroascorbic acid, which may be the reason for the good selectivity. More theoretical and experimental studies should be performed to provide more insights. An examination of the long-term stability of the fabricated electrode was carried out through the measurement of the current response to AA with the electrode stored under dry conditions. Following a month of storage, the sensor maintained approximately 93% of its current response to AA, which showed its long-term stability. In addition, the stability of the fabricated sensor must be ascribed to the chemical stability of the Ni_6MnO_8 nanoflakes in the alkaline solution. Five electrodes were prepared and subjected to the same conditions for the purpose of investigating the reproducibility of the developed sensor. It was found that the relative standard deviation (R.S.D.) was no more than 4.0% for these electrodes. With one sensor, the mean steady-state current had relative standard deviation of 6.2% for repeatedly detecting 0.1 mM AA six times, indicating good repeatability. To confirm the practical application of the prepared sensor, the analysis of the current response of the manufactured electrode to vitamin C tablets was carried out. The vitamin C tablets were purchased from a domestic drugstore. In accordance with the label, each of the tablets possessed 100 mg of AA. With regard to the analysis, the standard addition approach was used, with the help of which an established quantity of AA in water was introduced to the test solution. The recoveries determined for AA ranged between 96.5 percent and 99.3 percent, which is presented in Table 2. This result is a clear manifestation of the fact that the Ni_6MnO_8 nanoflake layer-modified microneedle sensor can be applied for determining AA.

Conclusions

In the current research work, a simple hydrothermal reaction-calcination process was employed for the growth of Ni_6MnO_8 nanoflakes on a steel acupuncture needle coated with a carbon film. The product was directly applied as an active electrode and non-enzymatic electrochemical sensor for detecting AA. The outstanding electrochemical attributes found were elevated sensitivity, a low detection limit, a broad linear range, and long-term stability. The Ni_6MnO_8 nanoflake layer-modified microneedle sensor presented here has potential for the detection of low quantities of analytes or *in vivo* calculations.

Conflicts of interest

There are no conflicts to declare.

Acknowledgements

The present research work received the support of the Chongqing Research Program of Basic Research and Frontier Technology (Grant No. cstc2016jcyjA0125) and the Fundamental Research Funds for the Central Universities (Grant No. XDJK2018B033).

References

1 Y. G. Lee, B. X. Liao and Y. C. Weng, *RSC Adv.*, 2018, **8**, 37872–37879.
2 Z. Y. Yu, H. J. Li, J. H. Lu, X. M. Zhang, N. K. Liu and X. Zhang, *Electrochim. Acta*, 2015, **158**, 264–270.
3 G. H. Wu, Y. F. Wu, X. W. Liu, M. C. Rong, X. M. Chen and X. Chen, *Anal. Chim. Acta*, 2012, **745**, 33–37.
4 R. M. Mazhabi, L. Q. Ge, H. Jiang and X. M. Wang, *Biosens. Bioelectron.*, 2018, **107**, 54–61.
5 S. Y. Zhu, C. H. Lei, Y. Gao, J. Sun, H. W. Peng, H. Gao, R. X. Zhang, R. Wang, X. E. Zhao and H. Wang, *New J. Chem.*, 2018, **42**, 3851–3856.
6 J. Wang, M. Zhou, R. Dong, X. Cong, R. Zhang and X. Wang, *Electroanalysis*, 2014, **29**, 2483–2490.
7 F. Turak, R. Guzel and E. Dinc, *J. Food Drug Anal.*, 2016, **25**, 285–292.
8 Y. T. Shieh, Y. A. Chen, R. H. Lin, T. L. Wang and C. H. Yang, *Colloid Polym. Sci.*, 2012, **290**, 1451–1456.
9 N. K. Mogha, V. Sahu, M. Sharma, R. K. Sharma and D. T. Masram, *Appl. Biochem. Biotechnol.*, 2014, **174**, 1010–1020.
10 Y. Y. Yin, J. W. Zhao, L. R. Qin, Y. Yang and L. Z. He, *RSC Adv.*, 2016, **6**, 63358–63364.
11 W. Y. Zhai, C. X. Wang, P. Yu, Y. X. Wang and L. Q. Mao, *Anal. Chem.*, 2014, **86**, 12206–12213.
12 C. Xia, X. Y. Jun and W. Ning, *Sens. Actuators, B*, 2011, **153**, 434–438.
13 N. Pal, S. Banerjee and A. Bhaumik, *J. Colloid Interface Sci.*, 2018, **516**, 121–127.
14 B. D. Liu, L. Q. Luo, Y. P. Ding, X. J. Si, Y. L. Wei, X. Q. Ouyang and D. Xu, *Electrochim. Acta*, 2014, **142**, 336–342.
15 L. Qin, G. W. Bin, Z. X. Peng, L. H. Tao, D. M. Ling, Z. Z. Ping and W. Feng, *RSC Adv.*, 2018, **8**, 13401–13407.
16 C. Feng, X. Kou, B. Chen, G. Qian, Y. Sun and G. Lu, *Sens. Actuators, B*, 2017, **253**, 584–591.
17 L. Y. He, F. Y. Wang, Y. Chen and Y. Y. Liu, *Luminescence*, 2018, **33**, 145–152.
18 J. G. Lin and W. L. Chen, *Am. J. Chin. Med.*, 2008, **36**, 635–645.

19 J. Zhou, L. Tang, F. Yang, F. Liang, H. Wang, Y. Li and G. Zhang, *Analyst*, 2017, **142**, 4322–4329.
20 X. Niu, Z. Wen, X. Li, W. Zhao, X. Li, Y. Huang, Q. Li, G. Li and W. Sun, *Sens. Actuators, B*, 2018, **255**, 471–477.
21 C. B. Duan, J. W. Zhao, L. R. Qin, L. J. Yang and Y. C. Zhou, *Mater. Lett.*, 2017, **208**, 65–68.
22 A. P. Dral and J. E. ten Elshof, *Sens. Actuators, B*, 2018, **272**, 369–392.
23 J. Zhao, H. Liu and Q. Zhang, *Appl. Surf. Sci.*, 2017, **392**, 1097–1106.
24 C. B. Duan, J. W. Zhao, L. R. Qin, L. J. Yang and Y. C. Zhou, *Mater. Lett.*, 2017, **208**, 65–68.
25 D. Zhao, P. Yu, L. Wang, F. Sun, L. Zhao, C. Tian, W. Zhou and H. Fu, *Nano Res.*, 2017, **10**, 263–275.
26 N. Abbasi, M. Moradi, S. Hajati, M. A. Kiani and J. Toth, *J. Mol. Liq.*, 2017, **244**, 269–278.
27 A. Puangjan, S. Chaiyasith, S. Wichitpanya, S. Daengduang and S. Puttota, *J. Electroanal. Chem.*, 2016, **782**, 192–201.
28 A. Ejaz and S. Jeon, *Electrochim. Acta*, 2017, **245**, 742–751.
29 J. Zhao, Z. Yan, L. Qin, X. Feng and P. Wang, *Chem. Lett.*, 2014, **43**, 814–816.
30 L. Li, P. Zhang, Z. Li, D. Li, B. Han, L. Tu, B. Li, Y. Wang, L. Ren, P. Yang, S. Ke, S. Ye and W. Shi, *Nanotechnology*, 2019, **30**, 325501.
31 M. A. Zahed, S. C. Barman, Md. Sharifuzzaman, X. Xuan, J. S. Nah and J. Y. Park, *J. Electrochem. Soc.*, 2018, **165**, B840–B847.
32 Z. Xin, Y. Sha, W. He, H. Uyama, Q. Xie, Z. Lu and F. Yang, *Biosens. Bioelectron.*, 2013, **55**, 446–451.
33 Y. M. Ma, M. Zhao, B. Cai, W. Wang, Z. Ye and J. Huang, *Biosens. Bioelectron.*, 2014, **59**, 384–388.
34 Y. Wen, J. Xu, M. Liu, D. Li, L. Lu, R. Yue and H. He, *J. Electroanal. Chem.*, 2012, **674**, 71–82.
35 S. Cui, J. Zhang, Y. Ding, S. Gu, P. Hu and Z. Hu, *Sci. China Mater.*, 2017, **60**, 766–776.
36 L. R. Qin, L. Z. He, J. W. Zhao, B. L. Zhao, Y. Y. Yin and Y. Yang, *Sens. Actuators, B*, 2017, **240**, 779–784.
37 X. Luo, Z. Zhang, Q. Wan, K. Wub and N. Yang, *Electrochem. Commun.*, 2015, **61**, 89–92.
38 W. Huang, Y. Cao, Y. Chen, Y. Zhou and Q. Huang, *Appl. Surf. Sci.*, 2015, **359**, 221–226.
39 Y. V. M. Reddy, B. Sravani, H. Maseed, T. Łuczak, M. Osińska, L. SubramanyamSarma, V. V. S. S. Srikanth and G. Madhavi, *New J. Chem.*, 2018, **42**, 16891–16901.